

Energy stable and conservative dynamical low-rank approximation for the Su-Olson problem

Lena Baumann^a, Lukas Einkemmer^b, Christian Klingenberg^a, Jonas Kusch^c

^a*University of Wuerzburg, Department of Mathematics, Wuerzburg, Germany, lena.baumann@uni-wuerzburg.de (Lena Baumann), klingen@mathematik.uni-wuerzburg.de (Christian Klingenberg)*

^b*University of Innsbruck, Numerical Analysis and Scientific Computing, Innsbruck, Austria, lukas.einkemmer@uibk.ac.at*

^c*Norwegian University of Life Sciences, Scientific Computing, Ås, Norway, jonas.kusch@nmbu.no*

Abstract

Computational methods for thermal radiative transfer problems exhibit high computational costs and a prohibitive memory footprint when the spatial and directional domains are finely resolved. A strategy to reduce such computational costs is dynamical low-rank approximation (DLRA), which represents and evolves the solution on a low-rank manifold, thereby significantly decreasing computational and memory requirements. Efficient discretizations for the DLRA evolution equations need to be carefully constructed to guarantee stability while enabling mass conservation. In this work, we focus on the Su-Olson closure and derive a stable discretization through an implicit coupling of energy and radiation density. Moreover, we propose a rank-adaptive strategy to preserve local mass conservation. Numerical results are presented which showcase the accuracy and efficiency of the proposed method.

Keywords: thermal radiative transfer, Su-Olson closure, dynamical low-rank approximation, energy stability, mass conservation, rank adaptivity

1. Introduction

Numerically solving the radiative transfer equations is a challenging task, especially due to the high dimensionality of the solution's phase space. A common strategy to tackle this issue is to choose coarse numerical discretizations and mitigate numerical artifacts [20, 23, 27] which arise due to the insufficient resolution, see e.g. [3, 12, 1, 21, 33]. Despite the success of these approaches in a large number of applications, the requirement of picking user-determined and problem dependent tuning parameters can render them impracticable. Another approach to deal with the problem's high dimensionality is the use of model order reduction techniques. A reduced order method which is gaining a considerable amount of attention in the field of radiation transport is dynamical low-rank approximation (DLRA) [17] due to its ability to yield accurate solutions while not requiring an expensive offline training phase. DLRA's core idea is to represent and evolve the solution on the low-rank manifold of rank r functions. Past work in the area of radiative transfer has focused on asymptotic-preserving schemes [9, 8], mass conservation [29], stable discretizations [18], imposing boundary conditions [19, 15] and implicit time discretizations [30]. A discontinuous Galerkin discretization of the DLRA evolution equations for thermal radiative transfer has been proposed in [4].

A key building block of efficient, accurate and stable methods for DLRA is the construction of time integrators which are robust irrespective of small singular values in the solution [16]. Three integrators which move on the low-rank manifold while not being restricted by its curvature are the *projector-splitting* (PS) integrator [22], the *basis update & Galerkin* (BUG) integrator [7], and the *parallel* integrator [6]. Since the PS integrator evolves one of the required subflows backward in time, the BUG and parallel integrator are preferable for diffusive problems while facilitating the construction of stable numerical discretization for

hyperbolic problems [18]. Moreover, the BUG integrator allows for a basis augmentation step [5] which can be used to construct conservative schemes for the Schrödinger equation [5] and the Vlasov–Poisson equations [11].

In this work we propose an energy stable and mass conservative DLRA scheme for the thermal radiative transfer equations using the Su–Olson closure. The main novelties of this paper are:

- *A stable numerical scheme for thermal radiative transfer:* We show that conventional IMEX schemes fail to guarantee energy stability and therefore propose a scheme which advances radiation and energy implicitly in a coupled fashion.
- *A mass conservative and rank-adaptive integrator:* We employ the basis augmentation step from [5] as well as the conservative truncation step from [11] to guarantee local mass conservation and rank adaptivity. In contrast to [11] we do not need to impose conservation through a modified L -step equation, but solely use the basis augmentation strategy from [5].

Moreover, we demonstrate numerical experiments which underline the derived stability and conservation properties of the proposed method while showing significantly reduced computational costs and memory requirements.

This paper is structured as follows: After the introduction in Section 1, we review the background on thermal radiative transfer and dynamical low-rank approximation in Section 2. In Section 3 we present the evolution equations for the thermal radiative transfer equations when using the rank-adaptive BUG integrator. Section 4 discretizes the resulting equations in angle and space. The main method is presented in Section 5 where a stable time discretization is proposed. We discuss local mass conservation of the scheme in Section 6. Numerical experiments are demonstrated in Section 7.

2. Background

2.1. Thermal radiative transfer

In this work, we study radiation particles moving through and interacting with a background material. By absorbing particles, the material heats up and emits new particles which can in turn again interact with the background. This process is described by the thermal radiative transport equations

$$\begin{aligned} \frac{1}{c} \partial_t f(t, x, \mu) + \mu \partial_x f(t, x, \mu) &= \sigma(B(t, x) - f(t, x, \mu)), \\ \partial_t e(t, x) &= \sigma(\langle f(t, x, \cdot) \rangle_\mu - B(t, x)), \end{aligned}$$

where we omit boundary and initial conditions for now. This system can be solved for the radiation density (also called angular flux) $f(t, x, \mu)$ and the internal energy $e(t, x)$ of the background medium. Here, $x \in D \subset \mathbb{R}$ is the spatial variable and $\mu \in [-1, 1]$ denotes the directional (or velocity) variable. The opacity σ encodes the rate at which particles are absorbed by the medium and we use brackets $\langle \cdot \rangle_\mu, \langle \cdot \rangle_x$ to indicate an integration over the directional domain and the spatial domain, respectively. Moreover, the speed of light is denoted by c and the energy equilibrium is denoted by $B(T)$. It often is described by the Stefan–Boltzmann law

$$B(T) = acT^4,$$

where a is the radiation constant and T is the temperature. Different closures exist to determine a relation between the temperature T and the internal energy e . The Su–Olson closure $e(T) = B(T)$ yields a linear system for f and B , which reads

$$\frac{1}{c} \partial_t f(t, x, \mu) + \mu \partial_x f(t, x, \mu) = \sigma(B(t, x) - f(t, x, \mu)), \quad (1a)$$

$$\partial_t B(t, x) = \sigma(\langle f(t, x, \cdot) \rangle_\mu - B(t, x)). \quad (1b)$$

This system has been solved analytically and serves as a common benchmark for numerical considerations [32, 28, 25, 26, 24]. Constructing numerical schemes to solve the above equation is challenging. First, the potentially stiff opacity term has to be treated by an implicit time integration scheme. Second, for three-dimensional spatial domains the computational costs and memory requirements of finely resolved spatial and angular discretizations become prohibitive. To tackle the high dimensionality, we choose a dynamical low-rank approximation which we introduce in the following.

2.2. Dynamical low-rank approximation

The core idea of dynamical low-rank approximation is to represent and evolve the solution to a given equation $\partial_t f(t, x, \mu) = F(f(t, x, \mu))$ on the manifold of rank r functions

$$\mathcal{M}_r = \left\{ f \in L^2(D \times [-1, 1]) : f(x, \mu) = \sum_{i,j=1}^r X_i(x) S_{ij} V_j(\mu) \text{ with invertible } \mathbf{S} = (S_{ij}) \in \mathbb{R}^{r \times r}, \right. \\ \left. X_i \in L^2(D), V_j \in L^2([-1, 1]) \text{ and } \langle X_i, X_j \rangle_x = \delta_{ij}, \langle V_i, V_j \rangle_\mu = \delta_{ij} \right\}$$

at every time point t . That is, for a given t , we have

$$f(t, x, \mu) = \sum_{i,j=1}^r X_i(t, x) S_{ij}(t) V_j(t, \mu).$$

To restrict the solution dynamics onto the low-rank manifold \mathcal{M}_r , we need to determine the corresponding tangent space which at position f under the Gauge conditions $\langle \dot{X}_i, X_j \rangle_x = 0, \langle \dot{V}_i, V_j \rangle_\mu = 0$ reads

$$\mathcal{T}_f \mathcal{M}_r = \left\{ \delta f \in L^2(D \times [-1, 1]) : \delta f(x, \mu) = \sum_{i,j=1}^r \delta X_i(x) S_{ij} V_j(\mu) + X_i(x) \delta S_{ij} V_j(\mu) + X_i(x) S_{ij} \delta V_j(\mu) \right. \\ \left. \text{with } \delta S_{ij} \in \mathbb{R}, \delta X_i \in L^2(D), \delta V_j \in L^2([-1, 1]) \text{ and } \langle \delta X_i, X_j \rangle_x = 0, \langle \delta V_i, V_j \rangle_\mu = 0 \right\}.$$

Having defined the low-rank manifold and its corresponding tangent space, we now wish to determine $f(t, \cdot, \cdot) \in \mathcal{M}_r$ such that $\partial_t f(t, \cdot, \cdot) \in \mathcal{T}_f \mathcal{M}_r$ and $\|\partial_t f(t, \cdot, \cdot) - F(f(t, \cdot, \cdot))\|_{L^2(D \times [-1, 1])}$ is minimized. That is, one wishes to determine f such that

$$\langle \partial_t f(t, \cdot, \cdot) - F(f(t, \cdot, \cdot)), \delta f \rangle_{x, \mu} = 0 \quad \text{for all } \delta f \in \mathcal{T}_f \mathcal{M}_r. \quad (2)$$

The orthogonal projector onto the tangent plane $\mathcal{T}_f \mathcal{M}_r$ can be explicitly given as

$$P(f)F(f) = \sum_{j=1}^r \langle V_j, F(f) \rangle_\mu V_j - \sum_{i,j=1}^r X_i \langle X_i V_j, F(f) \rangle_{x, \mu} V_j + \sum_{i=1}^r X_i \langle X_i, F(f) \rangle_x.$$

With this definition at hand, we can reformulate (2) as

$$\partial_t f(t, x, \mu) = P(f(t, x, \mu))F(f(t, x, \mu)).$$

To evolve the solution in time according to the above equation is not trivial. Indeed standard time integration schemes suffer from the curvature of the low-rank manifold, which is proportional to the smallest singular value of the low-rank solution [17]. Three integrators which move along the manifold without suffering from its high curvature exist: The projector-splitting integrator [22], the BUG integrator [7], and the parallel integrator [6]. In this work, we will use the basis-augmented extension to the BUG integrator [5] which we explain in the following.

The rank-adaptive BUG integrator [5] updates and augments the bases $\{X_i\}, \{V_j\}$ in parallel in the first two steps. In the third step, a Galerkin step is performed for the augmented bases followed by a truncation step to a new rank r_1 . In detail, to evolve the distribution function from $f(t_0, x, \mu) = \sum_{i,j=1}^r X_i^0(x) S_{ij}^0 V_j^0(\mu)$ at time t_0 to $f(t_1, x, \mu) = \sum_{i,j=1}^r X_i^1(x) S_{ij}^1 V_j^1(\mu)$ at time $t_1 = t_0 + \Delta t$ the integrator performs the following steps:

1. **K-Step:** Write $K_j(t, x) = \sum_{i=1}^r X_i(t, x) S_{ij}(t)$ such that $f(t, x, \mu) = \sum_{j=1}^r K_j(t, x) V_j^0(\mu)$. Update and augment the basis $X_i^0(x)$ with $i = 1, \dots, r$ to $\hat{X}_i^1(x)$ with $i = 1, \dots, 2r$ by solving

$$\partial_t K_j(t, x) = \left\langle V_j^0, F \left(\sum_{i=1}^r K_i(t, x) V_i^0 \right) \right\rangle_\mu, \quad K_j(t_0, x) = \sum_{i=1}^r X_i^0(x) S_{ij}^0.$$

Retrieve $\hat{X}_i^1(x)$ through Gram Schmidt such that $[K_j(t_1, x), X_i^0] = \sum_{i=1}^{2r} \hat{X}_i^1(x) R_{ij}^1$. Note that R_{ij}^1 is discarded after this step. Compute $\hat{M}_{ki} = \langle \hat{X}_k^1, X_i^0 \rangle_x$.

2. **L-Step:** Write $L_i(t, \mu) = \sum_{j=1}^r S_{ij}(t) V_j(t, \mu)$ such that $f(t, x, \mu) = \sum_{i=1}^r X_i^0 L_i(t, \mu)$. Update and augment the basis $V_j^0(\mu)$ with $j = 1, \dots, r$ to $\hat{V}_j^1(\mu)$ with $j = 1, \dots, 2r$ by solving

$$\partial_t L_i(t, \mu) = \left\langle X_i^0, F \left(\sum_{j=1}^r X_j^0 L_j(t, \mu) \right) \right\rangle_x, \quad L_i(t_0, \mu) = \sum_{j=1}^r S_{ij}^0 V_j^0(\mu).$$

Retrieve $\hat{V}_j^1(\mu)$ through Gram Schmidt such that $[L_i(t_1, \mu), V_j^0(\mu)] = \sum_{j=1}^{2r} \hat{V}_j^1(\mu) R_{ij}^2$. Note that R_{ij}^2 is discarded after this step. Compute $\hat{N}_{\ell j} = \langle \hat{V}_\ell^1, V_j^0 \rangle_\mu$.

3. **S-Step:** Update S_{ij}^0 with $i, j = 1, \dots, r$ to \hat{S}_{ij}^1 with $i, j = 1, \dots, 2r$ by solving

$$\dot{\hat{S}}_{ij}(t) = \left\langle \hat{X}_i^1 \hat{V}_j^1, F \left(\sum_{\ell, k=1}^{2r} \hat{X}_\ell^1 \hat{S}_{\ell k}(t) \hat{V}_k^1 \right) \right\rangle_{x, \mu}, \quad \hat{S}_{ij}(t_0) = \hat{M}_{ik} S_{k\ell}^0 \hat{N}_{j\ell}.$$

4. **Truncation:** Let \hat{S}_{ij}^1 be the entries of the matrix $\hat{\mathbf{S}}^1$. Compute the singular value decomposition of $\hat{\mathbf{S}}^1 = \hat{\mathbf{P}} \hat{\mathbf{\Sigma}} \hat{\mathbf{Q}}^\top$ with $\hat{\mathbf{\Sigma}} = \text{diag}(\sigma_j)$. Given a tolerance ϑ , choose the new rank $r_1 \leq 2r$ as the minimal number such that

$$\left(\sum_{j=r_1+1}^{2r} \sigma_j^2 \right)^{1/2} \leq \vartheta.$$

Let \mathbf{S}^1 with entries S_{ij}^1 be the $r_1 \times r_1$ diagonal matrix with the r_1 largest singular values and let \mathbf{P}^1 with entries P_{ij}^1 and \mathbf{Q}^1 with entries Q_{ji}^1 contain the first r_1 columns of $\hat{\mathbf{P}}$ and $\hat{\mathbf{Q}}$, respectively. Set $X_i^1(x) = \sum_{i=1}^{2r} \hat{X}_i^1(x) P_{ij}^1$ for $i = 1, \dots, r_1$ and $V_j^1(\mu) = \sum_{j=1}^{2r} \hat{V}_j^1(\mu) Q_{ji}^1$ for $j = 1, \dots, r_1$.

The updated solution after one time step is then given by $f(t_1, x, \mu) = \sum_{i,j=1}^{r_1} X_i^1(x) S_{ij}^1 V_j^1(\mu)$. Note that we are not limited to augmenting with the old basis, which we will use to construct our scheme.

3. Dynamical low-rank approximation for Su-Olson

Let us now derive the evolution equations of the rank-adaptive BUG integrator for the thermal radiative transfer equations with Su-Olson closure. To simplify notation, all derivations are performed for the essentially one-dimensional slab geometry. However, the derivation trivially extends to higher dimensions. We

start from the thermal radiative transfer equations (1) with Su-Olson closure $e(T) = B(T)$, which yields

$$\partial_t f(t, x, \mu) + \mu \partial_x f(t, x, \mu) = \sigma(B(t, x) - f(t, x, \mu)), \quad (3a)$$

$$\partial_t B(t, x) = \sigma(\langle f(t, x, \cdot) \rangle_\mu - B(t, x)). \quad (3b)$$

Note that we leave out the speed of light by doing a rescaling of time $\tau = t/c$ and in an abuse of notation use t to denote τ in the remainder. For the dynamical low-rank approximation let us write

$$f(t, x, \mu) \approx \sum_{i,j}^r X_i(t, x) S_{ij}(t) V_j(t, \mu). \quad (4)$$

In the following, we use Einstein's sum convention when not stated otherwise to ensure compactness of notation. We start with considering the evolution equations for the particle density (3a). By evolving the solution along the subspaces $X_i(t, x) S_{ij}(t) V_j(t_0, \mu)$ and $X_i(t_0, x) S_{ij}(t) V_j(t, \mu)$ we can derive the evolution equations of the K - and L -step of the BUG integrator:

K-step: Let us rewrite f as

$$f(t, x, \mu) = K_j(t, x) V_j^0(\mu) \quad \text{with} \quad K_j(t, x) = X_i(t, x) S_{ij}(t), \quad (5)$$

where $\{V_j^0\}$ denotes the set of orthonormal basis functions for the velocity space that shall be kept fixed in this step. Plugging (5) into (3a) and projecting onto $V_k^0(\mu)$ we obtain

$$\partial_t K_k(t, x) = -\partial_x K_j(t, x) \langle V_k^0, \mu V_j^0 \rangle_\mu + \sigma(B(t, x) \langle V_k^0 \rangle_\mu - K_k(t, x)). \quad (6)$$

L-step: For the L -step, let us write f as

$$f(t, x, \mu) = X_i^0(x) L_i(t, \mu) \quad \text{with} \quad L_i(t, \mu) = S_{ij}(t) V_j(t, \mu), \quad (7)$$

where $\{X_i^0\}$ denotes the set of spatial orthonormal basis functions that shall be kept fixed in this step. Plugging (7) into (3a) and projecting onto $X_k^0(x)$ yields

$$\partial_t L_k(t, \mu) = -\mu \left\langle X_k^0, \frac{d}{dx} X_i^0 \right\rangle_x L_i(t, \mu) + \sigma(\langle X_k^0, B(t, \cdot) \rangle_x - L_k(t, \mu)). \quad (8)$$

Lastly, we derive the augmented Galerkin step of the rank-adaptive BUG integrator. We denote the time updated spatial basis augmented with X_i^0 as \hat{X}_i^0 . The augmented directional basis \hat{V}_i^0 is constructed in the corresponding way. Then, the augmented Galerkin step is constructed according to:

S-step: For the S -step of the dynamical low-rank approximation we use the initial condition $\hat{S}_{ij}(t_0) = \langle \hat{X}_i^1 X_\ell^0 \rangle_x S_{\ell k}(t_0) \langle \hat{V}_j^1 V_k^0 \rangle_\mu$ and evolve the solution along the subspace

$$f(t, x, \mu) = \sum_{i,j=1}^{2r} \hat{X}_i^1(x) \hat{S}_{ij}(t) \hat{V}_j^1(\mu).$$

Inserting this representation into (3a) and testing against \hat{X}_k^1 and \hat{V}_ℓ^1 gives

$$\hat{S}_{k\ell}(t) = - \left\langle \hat{X}_k^1, \frac{d}{dx} \hat{X}_i^1 \right\rangle_x \hat{S}_{ij}(t) \langle \hat{V}_\ell^1, \mu \hat{V}_j^1 \rangle_\mu + \sigma(\langle \hat{X}_k^1, B(t, \cdot) \rangle_x \langle \hat{V}_\ell^1 \rangle_\mu - \hat{S}_{k\ell}(t)). \quad (9)$$

For equation (3b) we obtain by inserting the updated dynamical low-rank approximation of f

$$\partial_t B(t, x) = \sigma(\langle \hat{X}_i^1(x) \hat{S}_{ij}(t) \hat{V}_j^1 \rangle_\mu - B(t, x)). \quad (10)$$

4. Angular and spatial discretization

Having derived the K -, L - and S -step of the rank-adaptive BUG integrator, we can now proceed with discretizing in angle and space. For the angular discretization, we describe $V_j^0(\mu)$, $\hat{V}_j^1(\mu)$ and $L_i(t, \mu)$ by a modal representation as follows

$$V_j^0(\mu) \simeq \sum_{n=0}^{N-1} V_{nj}^0 P_n(\mu), \quad \hat{V}_j^1(\mu) \simeq \sum_{n=0}^{N-1} \hat{V}_{nj}^1 P_n(\mu), \quad L_i(t, \mu) \simeq \sum_{n=0}^{N-1} L_{ni}(t) P_n(\mu),$$

where P_n are the normalized Legendre polynomials. When using this modal representation in the evolution equations of DLRA, we can use the fact that defining the flux matrix $\mathbf{A} \in \mathbb{R}^{N \times N}$ as $A_{mn} := \langle P_m, \mu P_n \rangle_\mu$ lets us write flux matrices as

$$\langle V_k^0, \mu V_j^0 \rangle_\mu = V_{km}^0 A_{mn} V_{jn}^0.$$

The evolution equations with angular discretization then read

$$\partial_t K_k(t, x) = -\partial_x K_j(t, x) V_{nj}^0 A_{mn} V_{mk}^0 + \sigma(B(t, x) V_{0k}^0 - K_k(t, x)), \quad (11a)$$

$$\dot{L}_{mk}(t) = -\left\langle X_k^0, \frac{d}{dx} X_i^0 \right\rangle_x L_{ni}(t) A_{mn} + \sigma(\langle X_k^0, B(t, \cdot) \rangle_x \delta_{m0} - L_{mk}(t)), \quad (11b)$$

$$\dot{\hat{S}}_{k\ell}(t) = -\left\langle \hat{X}_k^1, \frac{d}{dx} \hat{X}_i^1 \right\rangle_x S_{ij}(t) \hat{V}_{nj}^1 A_{mn} \hat{V}_{m\ell}^1 + \sigma(\langle \hat{X}_k^1, B(t, \cdot) \rangle_x \hat{V}_{0\ell}^1 - \hat{S}_{k\ell}(t)). \quad (11c)$$

For the angular discretization of (10) we get

$$\partial_t B(t, x) = \sigma(\hat{X}_i^1(x) \hat{S}_{ij}(t) \hat{V}_{0j}^1 - B(t, x)). \quad (11d)$$

To derive a spatial discretization we choose a spatial grid $x_1 < \dots < x_{n_x}$ with equidistant spacing Δx . The solution in a given cell p is then represented according to

$$X_{pk}(t) \approx \frac{1}{\Delta x} \int_{x_p}^{x_{p+1}} X_k(t, x) dx, \quad K_{pk}(t) \approx \frac{1}{\Delta x} \int_{x_p}^{x_{p+1}} K_k(t, x) dx, \quad B_p(t) \approx \frac{1}{\Delta x} \int_{x_p}^{x_{p+1}} B(t, x) dx.$$

Spatial derivatives are approximated and stabilized through the tridiagonal stencil matrices $\mathbf{D}^x \approx \partial_x$ and $\mathbf{D}^{xx} \approx \Delta x \partial_{xx}$ with entries

$$D_{p,p\pm 1}^x = \frac{\pm 1}{2\Delta x}, \quad D_{p,p}^{xx} = -\frac{1}{\Delta x}, \quad D_{p,p\pm 1}^{xx} = \frac{1}{2\Delta x}.$$

Then, $\mathbf{D}^x, \mathbf{D}^{xx} \in \mathbb{R}^{n_x \times n_x}$. Moreover, we denote the Roe matrix as $|\mathbf{A}| = \mathbf{Q}|\mathbf{M}|\mathbf{Q}^\top$, where $\mathbf{A} = \mathbf{Q}\mathbf{M}\mathbf{Q}^\top$ with \mathbf{Q} orthogonal and $\mathbf{M} = \text{diag}(\sigma_1, \dots, \sigma_n)$.

We then obtain the spatially and angular discretized matrix ODEs

$$\dot{K}_{pk}(t) = -D_{qp}^x K_{pj}(t) V_{nj}^0 A_{mn} V_{mk}^0 + D_{qp}^{xx} K_{pj}(t) V_{nj}^0 |A|_{mn} V_{mk}^0 + \sigma(B_p(t) V_{0k}^0 - K_{pk}(t)), \quad (12a)$$

$$\dot{L}_{mk}(t) = -A_{mn} L_{ni}(t) X_{pi}^0 D_{qp}^x X_{qk}^0 + |A|_{mn} L_{ni}(t) X_{pi}^0 D_{qp}^{xx} X_{qk}^0 + \sigma(\delta_{m0} B_p(t) X_{pk}^0 - L_{mk}(t)), \quad (12b)$$

$$\dot{\hat{S}}_{k\ell}(t) = -\hat{X}_{pk}^1 D_{pq}^x \hat{X}_{qi}^1 \hat{S}_{ij}(t) \hat{V}_{nj}^1 A_{mn} \hat{V}_{m\ell}^1 + \hat{X}_{pk}^1 D_{pq}^{xx} \hat{X}_{qi}^1 \hat{S}_{ij}(t) \hat{V}_{nj}^1 |A|_{mn} \hat{V}_{m\ell}^1 + \sigma(\hat{X}_{pk}^1 B_p(t) \hat{V}_{0\ell}^1 - \hat{S}_{k\ell}(t)). \quad (12c)$$

Lastly, we obtain from (11d) for the energy equilibrium B the spatially discretized equation

$$\dot{B}_p(t) = \sigma(\hat{X}_{pi}^1 \hat{S}_{ij}(t) \hat{V}_{0j}^1 - B_p(t)) = \sigma(u_{p0}^1(t) - B_p(t)), \quad (12d)$$

where we use the notation $\hat{X}_{pi}^1 \hat{S}_{ij}(t) \hat{V}_{mj}^1 =: u_{pm}^1(t)$. We can now show that the semi-discrete time-dependent system (12) is energy stable. For this, let us first note the following properties of the chosen spatial stencils:

Lemma 1 (Summation by parts). *Let $y, z \in \mathbb{R}^{n_x}$. Then the stencil matrices fulfill the following properties:*

$$y_p D_{pq}^x z_q = -z_p D_{pq}^x y_q, \quad z_p D_{pq}^x z_q = 0, \quad y_p D_{pq}^{xx} z_q = z_p D_{pq}^{xx} y_q.$$

Moreover, let $\mathbf{D}^+ \in \mathbb{R}^{n_x \times n_x}$ be defined as

$$D_{p,p}^+ = \frac{-1}{\sqrt{2\Delta x}}, \quad D_{p,p+1}^+ = \frac{1}{\sqrt{2\Delta x}}.$$

Then, $z_p D_{pq}^{xx} z_q = -\left(D_{pq}^+ z_q\right)^2$.

Proof. The assertions follow directly by plugging in the definitions of the stencil matrices:

$$\begin{aligned} y_p D_{pq}^x z_q &= \frac{\pm 1}{2\Delta x} y_p (z_{p+1} - z_{p-1}) = \frac{\pm 1}{2\Delta x} (y_{p-1} z_p - y_{p+1} z_p) = -z_p D_{pq}^x y_q, \\ z_p D_{pq}^x z_q &= -z_p D_{pq}^x z_q = 0, \\ y_p D_{pq}^{xx} z_q &= \frac{1}{2\Delta x} y_p z_p - \frac{1}{\Delta x} (y_p z_{p+1} + y_p z_{p-1}) = \frac{1}{2\Delta x} y_p z_p - \frac{1}{\Delta x} (y_{p-1} z_p + y_{p+1} z_p) = z_p D_{pq}^{xx} y_q, \\ z_p D_{pq}^{xx} z_q &= -\frac{1}{2\Delta x} (z_p^2 - 2z_p z_{p+1} + z_{p+1}^2) = -\frac{1}{2\Delta x} (z_p - z_{p+1})^2 =: -(D_{pq}^+ z_q)^2. \end{aligned}$$

□

With these properties at hand, we can now show dissipation of the energy

$$E(t) := \frac{1}{2} \|\mathbf{u}^1(t)\|_F^2 + \frac{1}{2} \|\mathbf{B}(t)\|_E^2,$$

where $\|\cdot\|_F$ denotes the Frobenius norm and $\|\cdot\|_E$ denotes the Euclidean norm.

Theorem 1. *The semi-discrete time-continuous system consisting of (12) is energy stable, that is $\dot{E}(t) \leq 0$.*

Proof. Let us start from the S -step in (12c)

$$\dot{\hat{S}}_{k\ell}(t) = -\hat{X}_{pk}^1 D_{pq}^x \hat{X}_{qi}^1 \hat{S}_{ij}(t) \hat{V}_{nj}^1 A_{mn} \hat{V}_{m\ell}^1 + \hat{X}_{pk}^1 D_{pq}^{xx} \hat{X}_{qi}^1 \hat{S}_{ij}(t) \hat{V}_{nj}^1 |A|_{mn} \hat{V}_{m\ell}^1 + \sigma \left(\hat{X}_{pk}^1(x) B_p(t) \hat{V}_{0\ell}^1 - \hat{S}_{k\ell}(t) \right).$$

We multiply with $\hat{X}_{\alpha k}^1 \hat{V}_{\beta\ell}^1$ and introduce the projections $P_{\alpha p}^{X,1} = \hat{X}_{\alpha k}^1 \hat{X}_{pk}^1$ and $P_{m\beta}^{V,1} = \hat{V}_{m\ell}^1 \hat{V}_{\beta\ell}^1$. With the notation $\hat{X}_{qi}^1 \hat{S}_{ij}(t) \hat{V}_{nj}^1 = u_{qn}^1(t)$ we get

$$\dot{u}_{\alpha\beta}^1(t) = -P_{\alpha p}^{X,1} D_{pq}^x u_{qn}^1(t) A_{mn} P_{m\beta}^{V,1} + P_{\alpha p}^{X,1} D_{pq}^{xx} u_{qn}^1(t) |A|_{mn} P_{m\beta}^{V,1} + \sigma \left(P_{\alpha p}^{X,1} B_p(t) \delta_{0m} P_{m\beta}^{V,1} - u_{\alpha\beta}^1(t) \right).$$

Next, we multiply with $u_{\alpha\beta}^1(t)$ and sum over α and β . Note that

$$P_{\alpha p}^{X,1} u_{\alpha\beta}^1 = u_{p\beta}^1 \quad \text{and} \quad P_{m\beta}^{V,1} u_{p\beta}^1 = u_{pm}^1.$$

This leads to

$$\frac{1}{2} \frac{d}{dt} \|\mathbf{u}^1(t)\|_F^2 = -u_{pm}^1(t) D_{pq}^x u_{qn}^1(t) A_{mn} + u_{pm}^1(t) D_{pq}^{xx} u_{qn}^1(t) |A|_{mn} + \sigma \left(u_{pm}^1(t) B_p(t) \delta_{0m} - \|\mathbf{u}^1(t)\|^2 \right).$$

Recall that we can write $\mathbf{A} = \mathbf{Q}\mathbf{M}\mathbf{Q}^\top$ with $\mathbf{M} = \text{diag}(\sigma_1, \dots, \sigma_N)$. Inserting this representation gives

$$\begin{aligned} \frac{1}{2} \frac{d}{dt} \|\mathbf{u}^1(t)\|_F^2 &= -u_{pm}^1(t) D_{pq}^x u_{qn}^1(t) Q_{nk} \sigma_k Q_{mk} + u_{pm}^1(t) D_{pq}^{xx} u_{qn}^1(t) Q_{nk} |\sigma_k| Q_{mk} + (u_{pm}^1(t) B_p(t) \delta_{0m} - \|\mathbf{u}^1(t)\|^2) \\ &= -\sigma_k \tilde{u}_{pk}^1(t) D_{pq}^x \tilde{u}_{qk}^1(t) + |\sigma_k| \tilde{u}_{pk}^1(t) D_{pq}^{xx} \tilde{u}_{qk}^1(t) + (u_{pm}^1(t) B_p(t) \delta_{0m} - \|\mathbf{u}^1(t)\|^2), \end{aligned}$$

where $\tilde{u}_{pk}^1(t) = u_{pm}^1(t)Q_{mk}$. With the properties of the stencil matrices we get

$$\frac{1}{2} \frac{d}{dt} \|\mathbf{u}^1(t)\|_F^2 = - \left(D_{pq}^+ u_{qm}^1(t) |A|_{mn}^{1/2} \right)^2 + \sigma (u_{p0}(t) B_p(t) - \|\mathbf{u}^1(t)\|_F^2). \quad (13)$$

Next we consider equation (12d). Multiplication with $B_p(t)$ and summation over p gives

$$\frac{1}{2} \frac{d}{dt} \|\mathbf{B}(t)\|_E^2 = \sigma (u_{p0}(t) B_p(t) - \|\mathbf{B}(t)\|_E^2). \quad (14)$$

For the total energy of the system it holds that $E(t) = \frac{1}{2} \|\mathbf{u}^1(t)\|_F^2 + \frac{1}{2} \|\mathbf{B}(t)\|_E^2$. Adding the evolution equations (13) and (14) we get

$$\begin{aligned} \frac{d}{dt} E(t) &= - \left(D_{pq}^+ u_{qm}^1(t) |A|_{mn}^{1/2} \right)^2 + \sigma (u_{p0}^1(t) B_p(t) - \|\mathbf{u}^1(t)\|_F^2) + \sigma (u_{p0}^1(t) B_p(t) - \|\mathbf{B}(t)\|_E^2) \\ &= - \left(D_{pq}^+ u_{qm}^1(t) |A|_{mn}^{1/2} \right)^2 - \sigma ((u_{p0}^1(t) - B_p(t))^2 + (u_{pm}^1(t))^2 (1 - \delta_{m0})), \end{aligned}$$

where we rewrote $\|\mathbf{B}(t)\|_E^2 = B_p(t)^2$ and $\|\mathbf{u}^1(t)\|_F^2 = (u_{pm}^1(t))^2$. This expression is strictly negative which means that E is dissipated in time. Hence, the system is energy stable. \square

5. Time discretization

Our goal is to construct a conservative DLRA scheme which is energy stable under a sharp time step restriction. Constructing time discretization schemes which preserve the energy dissipation shown in Theorem 1 while not suffering from the potentially stiff opacity term is not trivial. In fact a classical IMEX scheme potentially will increase the total energy, which we demonstrate in the following.

5.1. Naive time discretization

We start from system (12) which still depends continuously on the time t . For the time discretization we choose a standard IMEX scheme and perform a splitting of energy and radiation transport equation. That is, we use an explicit Euler step for the transport part of the evolution equations, treat the energy equilibrium B explicitly and use an implicit Euler step for the scattering term. Note that the scheme describes the evolution from time t_0 to time $t_1 = t_0 + \Delta t$ but holds for all further time steps equivalently. This yields the fully discrete scheme

$$K_{pk}^1 = K_{pk}^0 - \Delta t D_{qp}^x K_{pj}^0 V_{nj}^0 A_{mn} V_{mk}^0 + \Delta t D_{qp}^{xx} K_{pj}^0 V_{nj}^0 |A|_{mn} V_{mk}^0 + \sigma (\Delta t B_p^0 V_{0k}^0 - \Delta t K_{pk}^1), \quad (15a)$$

$$L_{mk}^1 = L_{mk}^0 - \Delta t X_{qk}^0 D_{qp}^x X_{pi}^0 L_{ni}^0 A_{mn} + \Delta t X_{qk}^0 D_{qp}^{xx} X_{pi}^0 L_{ni}^0 |A|_{mn} + \sigma (\Delta t X_{pk}^0 B_p^0 \delta_{m0} - \Delta t L_{mk}^1). \quad (15b)$$

The time updated bases \hat{X}_{pk}^1 and \hat{V}_{pk}^1 are then retrieved through a QR-decomposition of the augmented bases $[K_{pk}^1, X_{pk}^0]$ and $[L_{pk}^1, V_{pk}^0]$ according to the rank-adaptive BUG integrator [5]. Lastly, we perform a Galerkin step for the augmented bases according to

$$\begin{aligned} \hat{S}_{k\ell}^1 &= \tilde{S}_{k\ell}^0 - \Delta t \hat{X}_{pk}^1 D_{pq}^x \hat{X}_{qi}^1 \tilde{S}_{ij}^0 \hat{V}_{nj}^1 A_{mn} \hat{V}_{m\ell}^1 + \Delta t \hat{X}_{pk}^1 D_{pq}^{xx} \hat{X}_{qi}^1 \tilde{S}_{ij}^0 \hat{V}_{nj}^1 |A|_{mn} \hat{V}_{m\ell}^1 \\ &\quad + \sigma (\Delta t \hat{X}_{pk}^1 B_p^0 \hat{V}_{0\ell}^1 - \Delta t \hat{S}_{k\ell}^1), \end{aligned} \quad (15c)$$

where $\tilde{S}_{k\ell}^0 := \hat{X}_{pk}^1 X_{pk}^0 S_{k\ell}^0 V_{m\ell}^0 \hat{V}_{m\ell}^1$. The energy is then updated via

$$B_p^1 = B_p^0 + \sigma \Delta t (\hat{X}_{pi}^1 \hat{S}_{ij}^1 \hat{V}_{0j}^1 - B_p^1). \quad (15d)$$

However, this numerical method has the undesirable property that it can increase the total energy during a time step. In Theorem 2 we show this analytically. This behavior is, obviously, completely unphysical.

Theorem 2. *There exist initial value pairs (u^0, B^0) and time step sizes Δt such that the naive scheme (15) results in (u^1, B^1) for which the energy increases, i.e. for which $E^1 > E^0$.*

Proof. Let us multiply the S -step (15c) with $\hat{X}_{\alpha k}^1 \hat{V}_{\beta \ell}^1$ and sum over α and β . Again we make use of the projections $P_{\alpha p}^{X,1} = \hat{X}_{\alpha k}^1 \hat{X}_{pk}^1$ and $P_{m\beta}^{V,1} = \hat{V}_{m\ell}^1 \hat{V}_{\beta \ell}^1$. With the definition of $\tilde{S}_{k\ell}^0$ we obtain for $u_{\alpha\beta}^1 := \hat{X}_{\alpha k}^1 \hat{S}_{k\ell}^1 \hat{V}_{\beta \ell}^1$

$$u_{\alpha\beta}^1 = u_{pm}^0 - P_{\alpha p}^{X,1} \Delta t D_{pq}^x u_{qn}^0 A_{mn} P_{m\beta}^{V,1} + P_{\alpha p}^{X,1} \Delta t D_{pq}^{xx} u_{qn}^0 |A|_{mn} P_{m\beta}^{V,1} + \sigma \left(\Delta t P_{\alpha p}^{X,1} B_p^0 \delta_{m0} P_{m\beta}^{V,1} - \Delta t u_{\alpha\beta}^1 \right). \quad (16)$$

Let us choose a constant solution in space, i.e., $B_j^1 = B^1$ and $u_{jk}^1 = u^1 \delta_{k0}$ for all spatial indices j . The scalar values B^1 and u^1 are chosen such that $B^1 = u_0^1 + \alpha$ where

$$0 < \alpha < \frac{\sigma \Delta t}{1 + \sigma \Delta t + \sigma^2 \Delta t^2 + \frac{1}{2} \sigma^3 \Delta t^3} u_0^1.$$

We can now verify that we obtain our chosen values for B_j^1 and u_{jk}^1 after a single step of (16) when using the initial condition

$$B^0 = B^1 + \sigma \Delta t \alpha = u_0^1 + \alpha(1 + \sigma \Delta t), \quad (17a)$$

$$u_0^0 = u_0^1 + \sigma \Delta t (u_0^1 - B^0) = u_0^1 - \sigma \Delta t \alpha (1 + \sigma \Delta t). \quad (17b)$$

To show this, note that since the solution is constant in space, all stencil terms drop out and we are left with

$$u_{\alpha\beta}^1 = u_{pm}^0 + \sigma \left(\Delta t P_{\alpha p}^{X,1} B_p^0 \delta_{m0} P_{m\beta}^{V,1} - \Delta t u_{\alpha\beta}^1 \right). \quad (18)$$

Since B_p^0 is constant in space and δ_{m0} lies in the span of our basis, we know that all projections in the above equation are exact. Plugging the initial values (17) into (18) we then directly obtain $u_{\alpha\beta}^1$. Similarly, by plugging (17) into (15d), we obtain B_p^1 .

Then, we square both of the initial terms (17) to get

$$\begin{aligned} (B^0)^2 &= (B^1)^2 + 2\sigma \Delta t \alpha B^1 + \sigma^2 \Delta t^2 \alpha^2 = (B^1)^2 + 2\sigma \Delta t \alpha (u_0^1 + \alpha) + \sigma^2 \Delta t^2 \alpha^2, \\ (u_0^0)^2 &= (u_0^1)^2 - 2\sigma \Delta t \alpha u_0^1 (1 + \sigma \Delta t) + \sigma^2 \Delta t^2 \alpha^2 (1 + \sigma \Delta t)^2. \end{aligned}$$

Adding these two terms and multiplying with $\frac{1}{2}$ yields

$$E^1 = E^0 + \sigma^2 \Delta t^2 \alpha u_0^1 - \sigma \Delta t \alpha^2 - \frac{1}{2} \sigma^2 \Delta t^2 \alpha^2 - \frac{1}{2} \sigma^2 \Delta t^2 \alpha^2 (1 + \sigma \Delta t)^2.$$

Note that $E^1 > E^0$ if

$$\sigma \Delta t u_0^1 - \alpha - \frac{1}{2} \sigma \Delta t \alpha - \frac{1}{2} \sigma \Delta t \alpha (1 + \sigma \Delta t)^2 > 0.$$

Rearranging gives

$$\alpha < \frac{\sigma \Delta t}{1 + \sigma \Delta t + \sigma^2 \Delta t^2 + \frac{1}{2} \sigma^3 \Delta t^3} u_0^1.$$

This is exactly the domain α is chosen from. Hence, we have $E^1 > E^0$, which is the desired result. \square

5.2. Energy stable space-time discretization

To construct an energy stable time integration scheme, we write the original equations in two parts followed by a basis augmentation and correction step. First, we evolve the basis functions according to

$$K_{pk}^* = K_{pk}^0 - \Delta t D_{qp}^x K_{pj}^0 V_{nj}^0 A_{mn} V_{mk}^0 + \Delta t D_{qp}^{xx} K_{pj}^0 V_{nj}^0 |A|_{mn} V_{mk}^0, \quad (19a)$$

$$L_{mk}^* = L_{mk}^0 - \Delta t X_{qk}^0 D_{qp}^x X_{pi}^0 L_{ni}^0 A_{mn} + \Delta t X_{qk}^0 D_{qp}^{xx} X_{pi}^0 L_{ni}^0 |A|_{mn}. \quad (19b)$$

We compute the augmented and time updated bases via QR-decompositions $\mathbf{X}^* \mathbf{R} = [\mathbf{K}^*, \mathbf{X}^0]$ and $\mathbf{V}^* \tilde{\mathbf{R}} = [\mathbf{L}^*, \mathbf{V}^0]$. With $\tilde{S}_{\alpha\beta}^0 = X_{j\alpha}^* X_{j\ell}^0 S_{\ell m}^0 V_{km}^0 V_{k\beta}^*$ we then solve the S -step equation

$$S_{\alpha\beta}^* = \tilde{S}_{\alpha\beta}^0 - \Delta t X_{p\alpha}^* D_{pq}^x X_{qi}^* \tilde{S}_{ij}^0 V_{nj}^* A_{mn} V_{m\beta}^* + \Delta t X_{p\alpha}^* D_{pq}^{xx} X_{qi}^* \tilde{S}_{ij}^0 V_{nj}^* |A|_{mn} V_{m\beta}^*. \quad (19c)$$

Second, we solve the coupled terms for the zeroth order moment and the energy according to

$$\hat{u}_{j0}^1 = X_{j\ell}^0 S_{\ell m}^0 V_{0m}^0 - \Delta t D_{ji}^x X_{in}^* \tilde{S}_{nm}^0 V_{\ell m}^* A_{0\ell} + \Delta t D_{ji}^{xx} X_{in}^* \tilde{S}_{nm}^0 V_{\ell m}^* |A|_{0\ell} + \sigma \Delta t (B_j^1 - \hat{u}_{j0}^1), \quad (19d)$$

$$B_j^1 = B_j^0 + \sigma \Delta t (\hat{u}_{j0}^1 - B_j^1). \quad (19e)$$

Following [18, Section 6] we perform the opacity update only on $\mathbf{L} = \mathbf{V}^* \mathbf{S}^*$ according to

$$L_{mk}^{*,\text{scat}} = \frac{1}{1 + \Delta t \sigma} L_{mk} \quad \text{for } k \neq 0 \quad (19f)$$

and retrieve the factorized basis and coefficients via a QR-decomposition $\mathbf{V}^{*,\text{scat}} \mathbf{S}^{*,\text{scat},\top} = \mathbf{L}^{*,\text{scat}}$.

Defining $\hat{\mathbf{u}}_0^1 = (\hat{u}_{j0}^1)_j$ we augment the basis matrices according to

$$\tilde{\mathbf{X}}^1 = \text{qr}([\hat{\mathbf{u}}_0^1, \mathbf{X}^*]), \quad \tilde{\mathbf{V}}^1 = \text{qr}([\mathbf{e}_1, \mathbf{V}^{*,\text{scat}}]). \quad (19g)$$

Third, the coefficient matrix is updated via

$$\tilde{\mathbf{S}}^1 = \tilde{\mathbf{X}}^{1,\top} \mathbf{X}^* \mathbf{S}^{*,\text{scat}} \mathbf{V}^{*,\text{scat},\top} (\mathbf{I} - \mathbf{e}_1 \mathbf{e}_1^\top) \tilde{\mathbf{V}}^1 + \tilde{\mathbf{X}}^{1,\top} \hat{\mathbf{u}}_0^1 \mathbf{e}_{1,\top} \tilde{\mathbf{V}}^1 \in \mathbb{R}^{(2r+1) \times (2r+1)}. \quad (19h)$$

Lastly, we truncate the rank $2r + 1$ solution to a new rank r_1 using a suited truncation strategy such as proposed in [5] or the conservative truncation strategy of [11]. We show that the given scheme is energy stable and start with the following Lemma.

Lemma 2. *Let us denote $u_{jk}^1 := \tilde{X}_{j\alpha}^1 \tilde{S}_{\alpha\beta}^1 \tilde{V}_{k\beta}^1$. Under the time step restriction $\Delta t \leq \Delta x$ it holds*

$$\frac{\Delta t}{2} (D_{ji}^x u_{jk}^1 A_{k\ell} - D_{ji}^{xx} u_{jk}^1 |A|_{k\ell})^2 - (D_{ji}^+ u_{ik}^1 |A|_{k\ell}^{1/2})^2 \leq 0. \quad (20)$$

Proof. Following [18], we employ a Fourier analysis which allows us to write the stencil matrices $\mathbf{D}^{x,xx,+}$ in diagonal form. Let us define $\mathbf{E} \in \mathbb{C}^{n_x \times n_x}$ with entries

$$E_{k\alpha} = \sqrt{\Delta x} \exp(i\alpha\pi x_k), \quad k, \alpha = 1, \dots, n_x$$

with $i \in \mathbb{C}$ being the imaginary unit. Then, the matrix \mathbf{E} is orthonormal, i.e., $\mathbf{E}\mathbf{E}^H = \mathbf{E}^H\mathbf{E} = \mathbf{I}$ (the uppercase H denotes the complex transpose) and it diagonalizes the stencil matrices:

$$\mathbf{D}^{x,xx,+} \mathbf{E} = \mathbf{E} \mathbf{\Lambda}^{x,xx,+}. \quad (21)$$

The matrices $\mathbf{\Lambda}^{x,xx,+}$ are diagonal with entries

$$\begin{aligned} \lambda_{\alpha,\alpha}^x &= \frac{1}{2\Delta x} (e^{i\alpha\pi\Delta x} - e^{-i\alpha\pi\Delta x}) = \frac{i}{\Delta x} \sin(\omega_\alpha), \\ \lambda_{\alpha,\alpha}^{xx} &= \frac{1}{2\Delta x} (e^{i\alpha\pi\Delta x} - 2 + e^{-i\alpha\pi\Delta x}) = \frac{1}{\Delta x} (\cos(\omega_\alpha) - 1), \\ \lambda_{\alpha,\alpha}^+ &= \frac{1}{\sqrt{2\Delta x}} (e^{i\alpha\pi\Delta x} - 1) = \frac{1}{\sqrt{2\Delta x}} (\cos(\omega_\alpha) + i \sin(\omega_\alpha) - 1), \end{aligned}$$

where we use $\omega_\alpha := \alpha\pi\Delta x$. Moreover, recall that we can write $\mathbf{A} = \mathbf{Q}\mathbf{M}\mathbf{Q}^\top$ where $\mathbf{M} = \text{diag}(\sigma_1, \dots, \sigma_N)$. We then have with $\hat{u}_{jk} = E_{j\ell}u_{\ell m}Q_{mk}$

$$\begin{aligned} & \frac{\Delta t}{2} (D_{ji}^x u_{jk}^1 A_{k\ell} - D_{ji}^{xx} u_{jk}^1 |A|_{k\ell})^2 - \left(D_{ji}^+ u_{ik}^1 |A|_{k\ell}^{1/2} \right)^2 \\ &= \frac{\Delta t}{2} \left| \lambda_{jj}^x \hat{u}_{jk}^1 \sigma_k - \lambda_{jj}^{xx} \hat{u}_{jk}^1 |\sigma_k| \right|^2 - \left| \lambda_{jj}^+ \hat{u}_{jk}^1 |\sigma_k|^{1/2} \right|^2 \\ &\leq \left[\Delta t \left(\frac{|\sigma_k|^2}{\Delta x^2} \cdot |1 - \cos(\omega_j)| \right) - \frac{|\sigma_k|}{\Delta x} \cdot |1 - \cos(\omega_j)| \right] (\hat{u}_{jk}^1)^2. \end{aligned}$$

To ensure negativity, we must have

$$\Delta t \left(\frac{|\sigma_k|^2}{\Delta x^2} \cdot |1 - \cos(\omega_j)| \right) \leq \frac{|\sigma_k|}{\Delta x} \cdot |1 - \cos(\omega_j)|.$$

Hence, for $\Delta t \leq \frac{\Delta x}{|\sigma_k|}$ equation (20) holds. Since $|\sigma_k| \leq 1$, we have proven the Lemma. \square

We can now show energy stability of the proposed scheme:

Theorem 3. *Under the time step restriction $\Delta t \leq \Delta x$, the scheme (19) is energy stable, i.e.,*

$$\|\mathbf{B}^1\|_E^2 + \|\mathbf{X}^1 \mathbf{S}^1 \mathbf{V}^{1,\top}\|_F^2 \leq \|\mathbf{B}^0\|_E^2 + \|\mathbf{X}^0 \mathbf{S}^0 \mathbf{V}^{0,\top}\|_F^2. \quad (22)$$

Proof. First, we multiply (19e) with B_j^1 and sum over j . Then,

$$(B_j^1)^2 = B_j^0 B_j^1 + \sigma \Delta t (u_{j0}^1 B_j^1 - (B_j^1)^2).$$

Let us note that

$$B_j^0 B_j^1 = \frac{(B_j^1)^2}{2} + \frac{(B_j^0)^2}{2} - \frac{1}{2} (B_j^1 - B_j^0)^2.$$

Hence,

$$\frac{1}{2} (B_j^1)^2 = \frac{1}{2} (B_j^0)^2 - \frac{1}{2} (B_j^1 - B_j^0)^2 + \sigma \Delta t (u_{j0}^1 B_j^1 - (B_j^1)^2). \quad (23)$$

To obtain a similar expression for $(u_{jk}^1)^2$, we multiply (19c) with $X_{j\alpha}^* V_{k\beta}^*$ and sum over α and β . For simplicity of notation, let us define $u_{jk}^* := X_{j\alpha}^* S_{\alpha\beta}^* V_{k\beta}^*$ and $u_{jk}^0 := X_{j\alpha}^* \tilde{S}_{\alpha\beta}^0 V_{k\beta}^*$ as well as the projections $P_{jp}^X := X_{j\alpha}^* X_{p\alpha}^*$ and $P_{km}^V := V_{k\beta}^* V_{m\beta}^*$. Then, we obtain the system

$$u_{jk}^* = u_{jk}^0 - \Delta t P_{jp}^X D_{pq}^x u_{qn}^0 A_{mn} P_{km}^V + \Delta t P_{jp}^X D_{pq}^{xx} u_{qn}^0 |A|_{mn} P_{km}^V. \quad (24)$$

Next, we define $u_{jk}^1 := \tilde{X}_{j\alpha}^1 \tilde{S}_{\alpha\beta}^1 \tilde{V}_{k\beta}^1$ and note that by construction we have that

$$u_{jk}^1 = \frac{u_{jk}^* (1 - \delta_{k0})}{1 + \sigma \Delta t} + \hat{u}_{j0}^1 \delta_{k0}.$$

Hence, plugging in the schemes for u_{jk}^* and \hat{u}_{j0}^1 , that is, (24) and (19d) we get

$$\begin{aligned} (1 + \sigma \Delta t) u_{jk}^1 &= (u_{jk}^0 - \Delta t P_{jp}^X D_{pq}^x u_{qn}^0 A_{mn} P_{km}^V + \Delta t P_{jp}^X D_{pq}^{xx} u_{qn}^0 |A|_{mn} P_{km}^V) (1 - \delta_{k0}) \\ &\quad + \left(X_{j\ell}^0 S_{\ell m}^0 V_{0m}^0 - \Delta t D_{ji}^x X_{in}^* \tilde{S}_{nm}^0 V_{\ell m}^* A_{0\ell} + \Delta t D_{ji}^{xx} X_{in}^* \tilde{S}_{nm}^0 V_{\ell m}^* |A|_{0\ell} + \sigma \Delta t B_j^1 \right) \delta_{k0}. \end{aligned}$$

Let us note that $P_{km}^V P_{jp}^X u_{jk}^1 = u_{jk}^1$ for $k \neq 0$. Hence, multiplying the above equation with u_{jk}^1 and summing over j and k gives

$$\begin{aligned} \frac{1}{2} (u_{jk}^1)^2 &= \frac{1}{2} (u_{jk}^0)^2 - \frac{1}{2} (u_{jk}^1 - u_{jk}^0)^2 - \Delta t u_{jk}^1 D_{ji}^x u_{i\ell}^0 A_{k\ell} + \Delta t u_{jk}^1 D_{ji}^{xx} u_{i\ell}^0 |A|_{k\ell} \\ &\quad + \sigma \Delta t u_{jk}^1 (B_j^1 \delta_{k0} - u_{jk}^1). \end{aligned}$$

Let us now add the zero term $\Delta t u_{jk}^1 D_{ji}^x u_{i\ell}^1 A_{k\ell}$ and add and subtract $\Delta t u_{jk}^1 D_{ji}^{xx} u_{i\ell}^1 |A|_{k\ell}$. Then,

$$\begin{aligned} \frac{1}{2} (u_{jk}^1)^2 &= \frac{1}{2} (u_{jk}^0)^2 - \frac{1}{2} (u_{jk}^1 - u_{jk}^0)^2 - \Delta t u_{jk}^1 D_{ji}^x (u_{i\ell}^0 - u_{i\ell}^1) A_{k\ell} \\ &\quad + \Delta t u_{jk}^1 D_{ji}^{xx} (u_{i\ell}^0 - u_{i\ell}^1) |A|_{k\ell} + \Delta t u_{jk}^1 D_{ji}^{xx} u_{i\ell}^1 |A|_{k\ell} \\ &\quad + \sigma \Delta t u_{jk}^1 (B_j^1 \delta_{k0} - u_{jk}^1). \end{aligned}$$

In the following, we use Young's inequality which states that for $a, b \in \mathbb{R}$ we have $a \cdot b \leq \frac{a^2}{2} + \frac{b^2}{2}$. We now apply this to the term

$$\begin{aligned} &-\Delta t u_{jk}^1 D_{ji}^x (u_{i\ell}^0 - u_{i\ell}^1) A_{k\ell} + \Delta t u_{jk}^1 D_{ji}^{xx} (u_{i\ell}^0 - u_{i\ell}^1) |A|_{k\ell} \\ &\leq \frac{1}{2} (u_{i\ell}^0 - u_{i\ell}^1)^2 + \frac{\Delta t^2}{2} (D_{ji}^x u_{jk}^1 A_{k\ell} - D_{ji}^{xx} u_{jk}^1 |A|_{k\ell})^2. \end{aligned}$$

Hence, using $u_{jk}^1 D_{ji}^{xx} u_{i\ell}^1 |A|_{k\ell} = - \left(D_{ji}^+ u_{ik}^1 |A|_{k\ell}^{1/2} \right)^2$ we get

$$\begin{aligned} \frac{1}{2} (u_{jk}^1)^2 &\leq \frac{1}{2} (u_{jk}^0)^2 + \frac{\Delta t^2}{2} (D_{ji}^x u_{jk}^1 A_{k\ell} - D_{ji}^{xx} u_{jk}^1 |A|_{k\ell})^2 - \Delta t \left(D_{ji}^+ u_{ik}^1 |A|_{k\ell}^{1/2} \right)^2 \\ &\quad + \sigma \Delta t u_{jk}^1 (B_j^1 \delta_{k0} - u_{jk}^1). \end{aligned} \quad (25)$$

As for the continuous case, we add (25) and (23) to obtain a time update equation for $E^0 := \frac{1}{2} (u_{jk}^0)^2 + \frac{1}{2} (B_j^0)^2$:

$$\begin{aligned} E^1 &\leq E^0 + \frac{\Delta t^2}{2} (D_{ji}^x u_{jk}^1 A_{k\ell} - D_{ji}^{xx} u_{jk}^1 |A|_{k\ell})^2 - \Delta t \left(D_{ji}^+ u_{ik}^1 |A|_{k\ell}^{1/2} \right)^2 \\ &\quad + \sigma \Delta t (u_{j0}^1 B_j^1 - (u_{jk}^1)^2) - \frac{1}{2} (B_j^1 - B_j^0)^2 + \sigma \Delta t (u_{j0}^1 B_j^1 - (B_j^1)^2) \\ &\leq E^0 + \frac{\Delta t^2}{2} (D_{ji}^x u_{jk}^1 A_{k\ell} - D_{ji}^{xx} u_{jk}^1 |A|_{k\ell})^2 - \Delta t \left(D_{ji}^+ u_{ik}^1 |A|_{k\ell}^{1/2} \right)^2 \\ &\quad - \sigma \Delta t (B_j^1 - u_{jk}^1)^2 - \frac{1}{2} (B_j^1 - B_j^0)^2. \end{aligned} \quad (26)$$

With Lemma 2 we have that

$$\frac{\Delta t}{2} (D_{ji}^x u_{jk}^1 A_{k\ell} - D_{ji}^{xx} u_{jk}^1 |A|_{k\ell})^2 - \left(D_{ji}^+ u_{ik}^1 |A|_{k\ell}^{1/2} \right)^2 \leq 0$$

for $\Delta t \leq \Delta x$. Since the truncation step is designed to not alter the zero order moments, we conclude that $E^1 \leq E^0$ and the full scheme is energy stable under the time step restriction $\Delta t \leq \Delta x$. \square

6. Mass conservation

Besides being energy stable, using a conservative truncation step ensures local conservation of mass. That is, we use the truncation strategy following [11, 14] which works as follows:

1. Compute $\tilde{\mathbf{K}} = \tilde{\mathbf{X}}^1 \tilde{\mathbf{S}}^1$ and split it into two parts $\tilde{\mathbf{K}} = [\tilde{\mathbf{K}}^{\text{cons}}, \tilde{\mathbf{K}}^{\text{rem}}]$ where $\tilde{\mathbf{K}}^{\text{cons}}$ corresponds to the first and $\tilde{\mathbf{K}}^{\text{rem}}$ consists of the remaining columns of $\tilde{\mathbf{K}}$. Analogously, distribute $\tilde{\mathbf{V}}^1 = [\tilde{\mathbf{V}}^{\text{cons}}, \tilde{\mathbf{V}}^{\text{rem}}]$ where $\tilde{\mathbf{V}}^{\text{cons}}$ corresponds to the first and $\tilde{\mathbf{V}}^{\text{rem}}$ consists of the remaining columns of $\tilde{\mathbf{V}}$.
2. Derive $\mathbf{X}^{\text{cons}} = \tilde{\mathbf{K}}^{\text{cons}} / \|\tilde{\mathbf{K}}^{\text{cons}}\|$ and $\mathbf{S}^{\text{cons}} = \|\tilde{\mathbf{K}}^{\text{cons}}\|$.
3. Perform a QR-decomposition of $\tilde{\mathbf{K}}^{\text{rem}}$ to obtain $\tilde{\mathbf{K}}^{\text{rem}} = \tilde{\mathbf{X}}^{\text{rem}} \tilde{\mathbf{S}}^{\text{rem}}$.
4. Compute the singular value decomposition of $\tilde{\mathbf{S}}^{\text{rem}} = \mathbf{U} \Sigma \mathbf{W}^\top$ with $\Sigma = \text{diag}(\sigma_j)$. Given a tolerance ϑ , choose the new rank $r_1 \leq 2r$ as the minimal number such that

$$\left(\sum_{j=r_1+1}^{2r} \sigma_j^2 \right)^{1/2} \leq \vartheta.$$

Let \mathbf{S}^{rem} be the $r_1 \times r_1$ diagonal matrix with the r_1 largest singular values and let \mathbf{U}^{rem} and \mathbf{W}^{rem} contain the first r_1 columns of \mathbf{U} and \mathbf{W} , respectively. Set $\mathbf{X}^{\text{rem}} = \tilde{\mathbf{X}}^{\text{rem}} \mathbf{U}^{\text{rem}}$ and $\mathbf{V}^{\text{rem}} = \tilde{\mathbf{V}}^{\text{rem}} \mathbf{W}^{\text{rem}}$.

5. Set $\hat{\mathbf{X}} = [\mathbf{X}^{\text{cons}}, \mathbf{X}^{\text{rem}}]$ and $\hat{\mathbf{V}} = [\mathbf{e}_1, \mathbf{V}^{\text{rem}}]$. Perform a QR-decomposition of $\hat{\mathbf{X}} = \mathbf{X}^1 \mathbf{R}^1$ and $\hat{\mathbf{V}} = \mathbf{V}^1 \mathbf{R}^2$.
6. Set

$$\mathbf{S}^1 = \mathbf{R}^1 \begin{bmatrix} \mathbf{S}^{\text{cons}} & 0 \\ 0 & \mathbf{S}^{\text{rem}} \end{bmatrix} \mathbf{R}^{2,\top}.$$

The updated solution at time $t_1 = t_0 + \Delta t$ is then given by $\mathbf{u}^1 = \mathbf{X}^1 \mathbf{S}^1 \mathbf{V}^{1,\top}$.

Then, the scheme is conservative:

Theorem 4. *The scheme (19) is locally conservative. That is, for the scalar flux at time t_n denoted by $\Phi_j^n = X_{j\ell}^n S_{\ell m}^n V_{0m}^n$, where $n \in \{0, 1\}$ and $u_{jk}^0 = X_{j\ell}^0 S_{\ell m}^0 V_{km}^0$ it fulfills the conservation law*

$$\Phi_j^1 = \Phi_j^0 - \Delta t D_{ji}^x u_{i\ell}^0 A_{0\ell} + \Delta t D_{ji}^{xx} u_{i\ell}^0 |A|_{0\ell} + \sigma \Delta t (B_j^1 - \Phi_j^1), \quad (27a)$$

$$B_j^1 = B_j^0 + \sigma \Delta t (\Phi_j^1 - B_j^1). \quad (27b)$$

Proof. From the conservative truncation step and the basis augmentation (19h) we know that

$$\Phi_j^1 = \tilde{X}_{j\ell}^1 \tilde{S}_{\ell m}^1 \tilde{V}_{0m}^1 = \hat{u}_{j0}^1.$$

Hence, with (19d) and (19e) we get that

$$\begin{aligned} \Phi_j^1 &= X_{j\ell}^0 S_{\ell m}^0 V_{0m}^0 - \Delta t D_{ji}^x X_{in}^* \tilde{S}_{nm}^0 V_{\ell m}^* A_{0\ell} + \Delta t D_{ji}^{xx} X_{in}^* \tilde{S}_{nm}^0 V_{\ell m}^* |A|_{0\ell} + \sigma \Delta t (B_j^1 - \Phi_j^1), \\ B_j^1 &= B_j^0 + \sigma \Delta t (\Phi_j^1 - B_j^1). \end{aligned}$$

Since the basis augmentation with \mathbf{X}^0 and \mathbf{V}^0 ensures $X_{j\ell}^0 S_{\ell m}^0 V_{0m}^0 = X_{in}^* \tilde{S}_{nm}^0 V_{\ell m}^* = u_{i\ell}^0$, the local conservation law (27) holds. \square

Hence, equipped with a conservative truncation step, the energy stable algorithm presented in (19) conserves mass locally. To give an overview of the algorithm, we visualize the main steps in Figure 1.

7. Numerical results

In this section we give numerical results to validate the proposed DLRA algorithm. The source code to reproduce the presented numerical results is openly available, see [2].

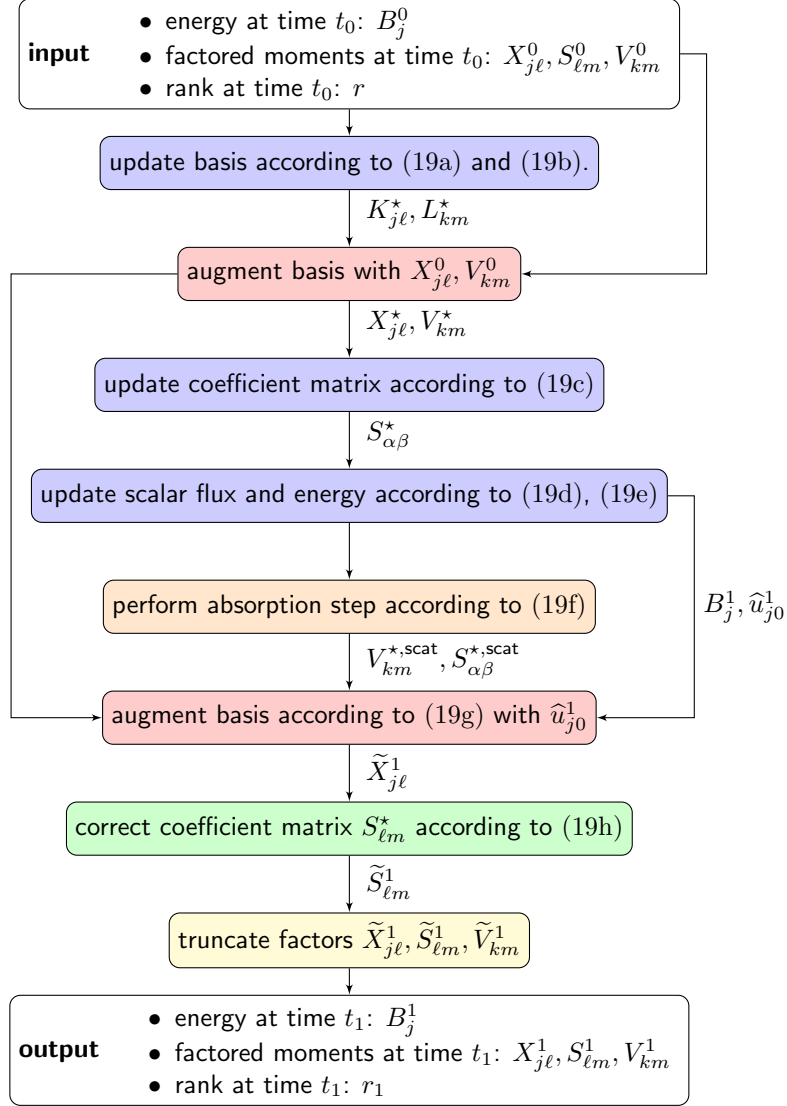


Figure 1: Flowchart of the stable and conservative method (19).

7.1. 1D Plane source

We consider the thermal radiative transfer equations as described in (3) on the spatial domain $D = [-10, 10]$. As initial distribution we choose a cutoff Gaussian

$$u(t=0, x) = \max \left(10^{-4}, \frac{1}{\sqrt{2\pi\sigma_{\text{IC}}^2}} \exp \left(-\frac{(x-1)^2}{2\sigma_{\text{IC}}^2} \right) \right),$$

with constant deviation $\sigma_{\text{IC}} = 0.03$. Particles are initially centered around $x = 1$ and move into all directions $\mu \in [-1, 1]$. The initial value for the energy equilibrium is set to $B^0 = 1$ and we start computations with a rank of $r = 20$. The opacity σ is set to the constant value of 1. Note that this setting is an extension of the so-called *plane source* problem, which is a common test case for the radiative transfer equation [13]. In the context of dynamical low-rank approximation it has been studied in [5, 18, 29, 31]. We compare the solution of the full coupled-implicit system without DLRA which reads

$$u_{jk}^1 = u_{jk}^0 - \Delta t D_{ji}^x u_{i\ell}^0 A_{k\ell} + \Delta t D_{ji}^{xx} u_{i\ell}^0 |A|_{k\ell} + \sigma \Delta t (B_j^1 \delta_{k0} - u_{jk}^1) \quad (28a)$$

$$B_j^1 = B_j^0 + \sigma \Delta t (u_{j0}^1 - B_j^1) \quad (28b)$$

to the presented energy stable mass conservative DLRA solution from (19). The total mass at any time t_n shall be defined as $m^n = \Delta x \sum_j (u_{j0}^n + B_j^n)$. As computational parameters we use $n_x = 1000$ cells in the spatial domain and $N = 500$ moments to represent the directional variable. The time step size is chosen as $\Delta t = \text{CFL} \cdot \Delta x$ with a CFL number of $\text{CFL} = 0.99$. In Figure 2 we present the full solution $f(x, \mu)$, the scalar flux $\Phi = \langle f \rangle_\mu$ and the temperature T at the end time $t_{\text{end}} = 8$. Further, the evolution of the rank r in time, and the relative mass error $\frac{|m^0 - m^n|}{\|m^0\|}$ are shown. One can observe that the DLRA scheme captures well the solution of the full system. For a chosen tolerance of $\vartheta = 10^{-1} \|\Sigma\|_2$ the rank increases up to $r = 24$ before it reduces again. The relative mass error is of order $\mathcal{O}(10^{-14})$. Hence, our proposed scheme is mass conservative up to machine precision.

7.2. 1D Su-Olson problem

For the next test problem we add a source term $Q(x)$ to the previously investigated equations leading to

$$\begin{aligned} \partial_t f(t, x, \mu) + \mu \partial_x f(t, x, \mu) &= \sigma (B(t, x) - f(t, x, \mu)) + Q(x), \\ \partial_t B(t, x) &= \sigma (\langle f(t, x, \cdot) \rangle_\mu - B(t, x)). \end{aligned}$$

In our example we use the source function $Q(x) = \chi_{[-0.5, 0.5]}(x)/a$ with $a = \frac{4\sigma_{\text{SB}}}{c}$ being the radiation constant depending on the Stefan-Boltzmann constant σ_{SB} and the speed of light c . Again we consider the spatial domain $D = [-10, 10]$ and choose the initial condition

$$u(t=0, x) = \max \left(10^{-4}, \frac{1}{\sqrt{2\pi\sigma_{\text{IC}}^2}} \exp \left(-\frac{(x-1)^2}{2\sigma_{\text{IC}}^2} \right) \right),$$

with constant deviation $\sigma_{\text{IC}} = 0.03$ and particles moving into all directions $\mu \in [-1, 1]$. The initial value for the energy equilibrium is set to $B_0 = 50$, the initial value for the rank to $r = 20$. The opacity σ is again chosen to have the constant value of 1. As computational parameters we use $n_x = 1000$ cells in the spatial domain and $N = 500$ moments to represent the directional variable. The time step size is chosen as $\Delta t = \text{CFL} \cdot \Delta x$ with a CFL number of $\text{CFL} = 0.99$. The isotropic source term generates radiation particles flying through and interacting with a background material. The interaction is driven by the opacity σ . In turn, particles heat up the material leading to a travelling temperature front, also called a *Marshak wave*. Again this travelling heat wave can lead to the emission of new particles from the background material generating a particle wave. At a given time point $t_{\text{end}} = 3.16$ this waves can be seen in Figure 3 where we display numerical results for the full solution $f(x, \mu)$, the scalar flux $\Phi = \langle f \rangle_\mu$ and the temperature T . We compare the solution of the full coupled-implicit system differing from (28) by an additional source term to the presented energy stable mass conservative DLRA solution from (19). Further, the evolution of the rank in time is presented for a tolerance parameter of $\vartheta = 10^{-2} \|\Sigma\|_2$. Note that due to the source term there is no mass conservation in this example.

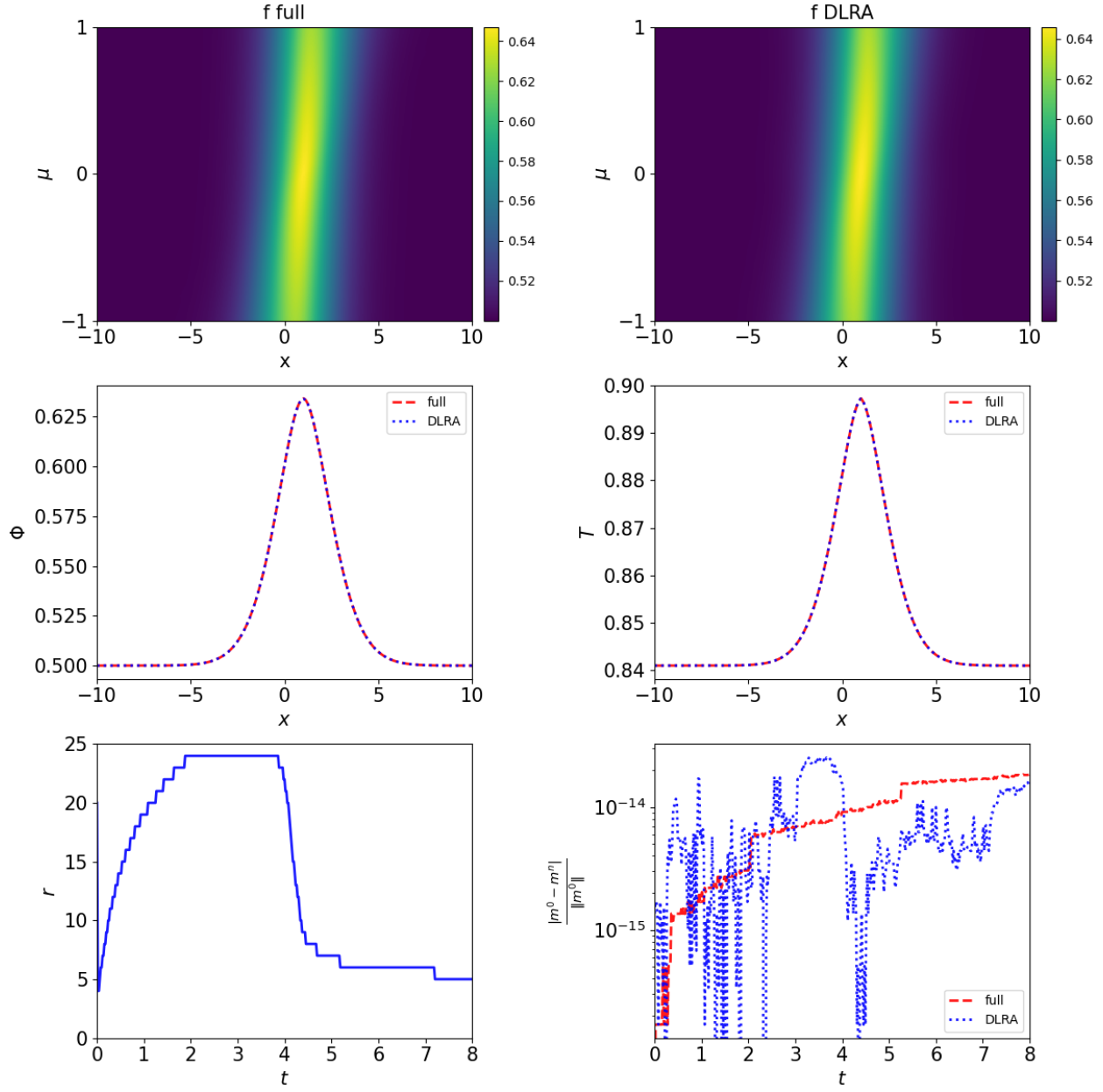


Figure 2: Top row: Numerical results for the full solution $f(x, \mu)$ of the plane source problem computed with the full coupled-implicit system (left) and the DLRA system (right). Middle row: Travelling particle (left) and heat wave (right) for both the full system and the DLRA system. Bottom row: Evolution of the rank in time for the DLRA method (left) and relative mass error compared for both methods (right).

7.3. 2D Beam

To approve computational benefits of the presented method we extend it to a two-dimensional setting. The set of equations becomes:

$$\begin{aligned}\partial_t f(t, \mathbf{x}, \Omega) + \Omega \cdot \nabla_{\mathbf{x}} f(t, \mathbf{x}, \Omega) &= \sigma(B(t, \mathbf{x}) - f(t, \mathbf{x}, \Omega)), \\ \partial_t B(t, \mathbf{x}) &= \sigma(\langle f(t, \mathbf{x}, \cdot) \rangle_{\Omega} - B(t, \mathbf{x})).\end{aligned}$$

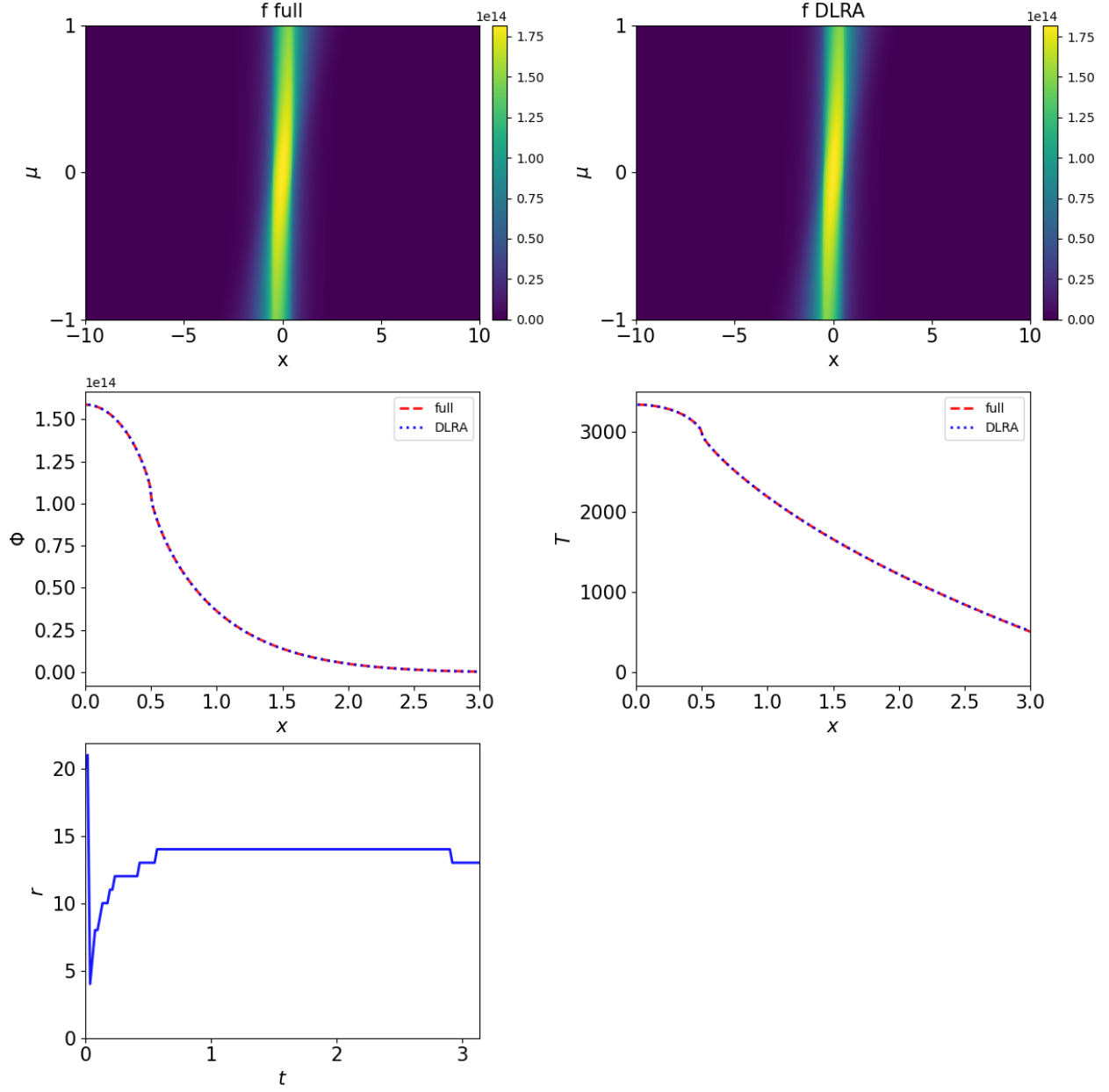


Figure 3: Top row: Numerical results for the full solution $f(x, \mu)$ of the Su-Olson problem computed with the full coupled-implicit system (left) and the DLRA system (right). Middle row: Travelling particle (left) and heat wave (right) for both the full system and the DLRA system. Bottom row: Evolution of the rank in time for the DLRA method.

For the numerical experiments let $\mathbf{x} = (x_1, x_2) \in [-1, 1] \times [-1, 1]$, $\boldsymbol{\Omega} = (\Omega_1, \Omega_2, \Omega_3) \in \mathcal{S}^2$ and $\sigma = 0.5$. The initial condition of the two-dimensional beam is given by

$$f(t=0, \mathbf{x}, \boldsymbol{\Omega}) = 10^6 \cdot \frac{1}{2\pi\sigma_x^2} \exp\left(-\frac{\|\mathbf{x}\|^2}{2\sigma_x^2}\right) \cdot \frac{1}{2\pi\sigma_\Omega^2} \exp\left(-\frac{(\Omega_1 - \Omega^*)^2 + (\Omega_3 - \Omega^*)^2}{2\sigma_\Omega^2}\right),$$

with $\Omega^* = \frac{1}{\sqrt{2}}$, $\sigma_x = \sigma_\Omega = 0.1$. The initial value for the energy equilibrium is set to $B^0 = 1$, the initial value for the rank to $r = 100$. The total mass at any time t_n shall be defined as $m^n = \Delta x_1 \Delta x_2 \sum_j (u_{j0}^n + B_j^n)$.

We perform our computations on a spatial grid with $N_{\text{CellsX}} = 500$ points in x_1 and $N_{\text{CellsY}} = 500$ points in x_2 . Further, we use a polynomial degree of $n_{\text{PN}} = 29$ corresponding to 900 expansion coefficients in angle. The time step size is chosen as $\Delta t = \text{CFL} \cdot \Delta x$ with a CFL number of $\text{CFL} = 0.7$.

We compare the solution of the two-dimensional full system corresponding to (28) to the two-dimensional DLRA solution corresponding to (19). In Figure 4 we show numerical results for the scalar flux $\Phi = \int_{S^2} f(t, \mathbf{x}, \cdot) d\Omega$ and the temperature T at the time $t = 0.5$. For this setup the computational benefit of the DLRA method is significant as the run time compared to the solution of the full problem is reduced by a factor of approximately 8 from 20023 seconds to 2509 seconds.

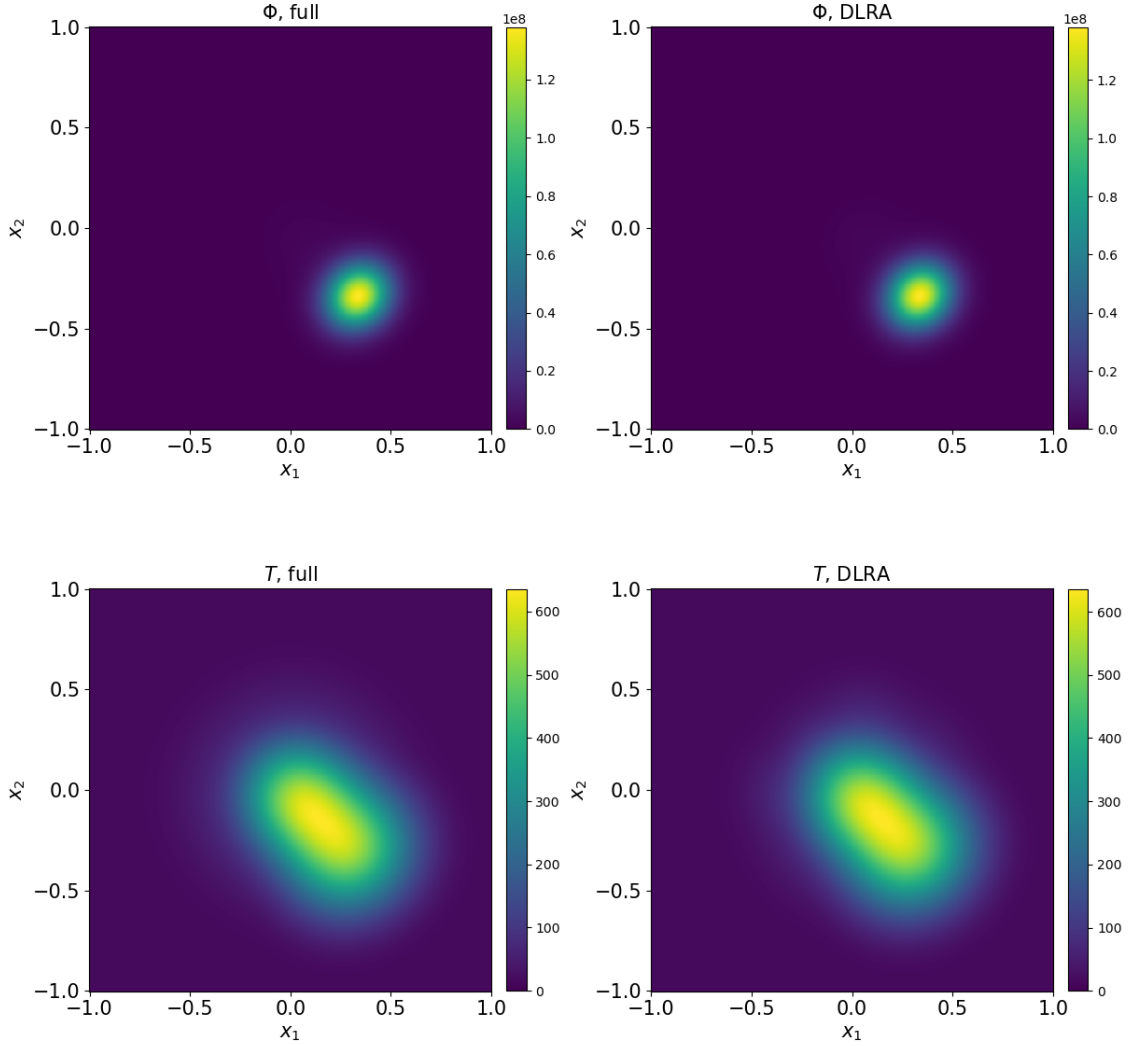


Figure 4: Numerical results of the scalar flux and the temperature for the 2D beam example for the full coupled-implicit system (left) and the DLRA system (right) at the time $t = 0.5$.

For the evolution of the rank r in time and the relative mass error $\frac{|m^0 - m^n|}{\|m^0\|}$ we consider a time interval up to $t = 1.5$. In Figure 5 one can observe that for a chosen tolerance parameter of $\vartheta = 5 \cdot 10^{-4} \|\Sigma\|_2$ the rank increases but does not approach its allowed maximal value of 100. Further, the relative mass error stagnates

and the DLRA method shows its mass conservation property.

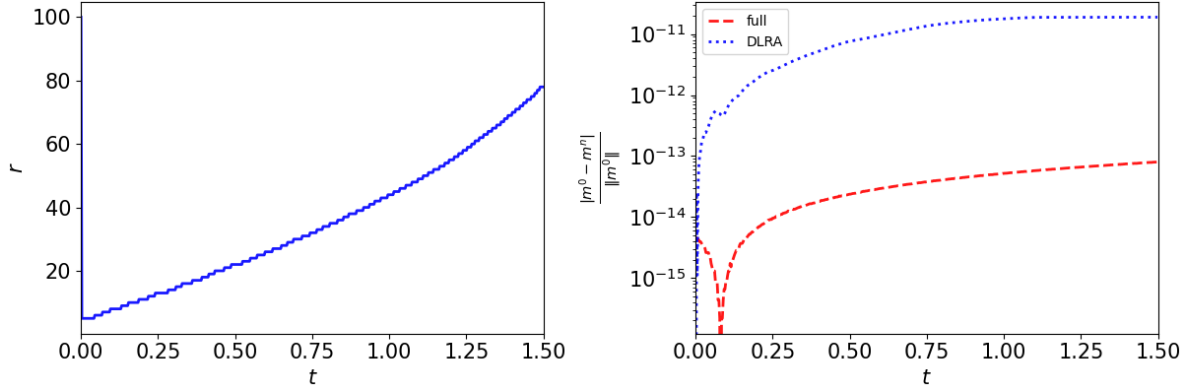


Figure 5: Evolution of the rank in time for the 2D beam example for the DLRA method (left) and relative mass error compared for both methods (right) until a time of $t = 1.5$.

8. Conclusion and outlook

We have introduced an energy stable and mass conservative dynamical low-rank algorithm for the Su-Olson problem. The key points leading to these properties consist in treating both equations in a coupled-implicit way and using a mass conservative truncation strategy. Numerical examples both in 1D and 2D validate the accuracy of the DLRA method. Its efficiency can especially be seen in the two-dimensional setting. For future work, we propose to implement the parallel integrator of [6] for further enhancing the efficiency of the DLRA method. Moreover, we expect to draw conclusions from this Su-Olson system to the Boltzmann-BGK system and the DLRA algorithm presented in [10] regarding stability and an appropriate choice of the size of the time step.

Acknowledgements

Lena Baumann acknowledges support by the Würzburg Mathematics Center for Communication and Interaction (WMCCI) as well as the Stiftung der Deutschen Wirtschaft. The work of Jonas Kusch was funded by the Deutsche Forschungsgemeinschaft (DFG, German Research Foundation) – 491976834.

Author Contribution Statement (CRediT)

Lena Baumann:	analysis of energy stability, conceptualization, implementation, plotting, simulation of numerical tests, validation, visualization, writing - original draft
Lukas Einkemmer:	analysis of energy stability, conceptualization, initial idea of numerical scheme, proofreading and corrections, supervision
Christian Klingenberg:	conceptualization, proofreading and corrections, supervision
Jonas Kusch:	analysis of energy stability, conceptualization, implementation, initial idea of numerical scheme, simulation/setup of numerical tests, supervision, visualization, writing - original draft

References

- [1] I. Abu-Shumays. Angular quadratures for improved transport computations. *Transport Theory and Statistical Physics*, 30(2-3):169–204, 2001.
- [2] L. Baumann, L. Einkemmer, C. Klingenberg, and J. Kusch. Numerical testcases for "Energy stable and conservative dynamical low-rank approximation for the Su-Olson problem". <https://github.com/JonasKu/publication-Energy-stable-and-conservative-dynamical-low-rank-approximation-for-the-Su-Olson-problem.git>, 2023.
- [3] T. Camminady, M. Frank, K. Küpper, and J. Kusch. Ray effect mitigation for the discrete ordinates method through quadrature rotation. *Journal of Computational Physics*, 382:105–123, 2019.
- [4] G. Ceruti, M. Frank, and J. Kusch. Dynamical low-rank approximation for Marshak waves. CRC 1173 Preprint 2022/76, Karlsruhe Institute of Technology, 2022.
- [5] G. Ceruti, J. Kusch, and C. Lubich. A rank-adaptive robust integrator for dynamical low-rank approximation. *BIT Numerical Mathematics*, 62:1149–1174, 2022.
- [6] G. Ceruti, J. Kusch, and C. Lubich. A parallel rank-adaptive integrator for dynamical low-rank approximation. *arXiv preprint arXiv:2304.05660*, 2023.
- [7] G. Ceruti and C. Lubich. An unconventional robust integrator for dynamical low-rank approximation. *BIT Numerical Mathematics*, 62(1):23–44, 2022.
- [8] L. Einkemmer, J. Hu, and J. Kusch. Asymptotic-preserving and energy stable dynamical low-rank approximation. *arXiv preprint arXiv:2212.12012*, 2022.
- [9] L. Einkemmer, J. Hu, and Y. Wang. An asymptotic-preserving dynamical low-rank method for the multi-scale multi-dimensional linear transport equation. *Journal of Computational Physics*, 439:110353, 2021.
- [10] L. Einkemmer, J. Hu, and L. Ying. An efficient dynamical low-rank algorithm for the Boltzmann-BGK equation close to the compressible viscous flow regime. *SIAM Journal on Scientific Computing*, 43(5):B1057–B1080, 2021.
- [11] L. Einkemmer, A. Ostermann, and C. Scalone. A robust and conservative dynamical low-rank algorithm. *arXiv preprint arXiv:2206.09374*, 2022.
- [12] M. Frank, J. Kusch, T. Camminady, and C. D. Hauck. Ray effect mitigation for the discrete ordinates method using artificial scattering. *Nuclear Science and Engineering*, 194(11):971–988, 2020.
- [13] B. D. Ganapol. Analytical benchmarks for nuclear engineering applications. *Case Studies in Neutron Transport Theory*, 2008.
- [14] W. Guo and J.-M. Qiu. A conservative low rank tensor method for the Vlasov dynamics. *arXiv preprint arXiv:2201.10397*, 2022.
- [15] J. Hu and Y. Wang. An adaptive dynamical low rank method for the nonlinear Boltzmann equation. *Journal of Scientific Computing*, 92(2):75, 2022.
- [16] E. Kieri, C. Lubich, and H. Walach. Discretized dynamical low-rank approximation in the presence of small singular values. *SIAM Journal on Numerical Analysis*, 54(2):1020–1038, 2016.
- [17] O. Koch and C. Lubich. Dynamical low-rank approximation. *SIAM Journal on Matrix Analysis and Applications*, 29(2):434–454, 2007.
- [18] J. Kusch, L. Einkemmer, and G. Ceruti. On the stability of robust dynamical low-rank approximations for hyperbolic problems. *SIAM Journal on Scientific Computing*, 45(1):A1–A24, 2023.
- [19] J. Kusch and P. Stammer. A robust collision source method for rank adaptive dynamical low-rank approximation in radiation therapy. *ESAIM: M2AN*, 2022.
- [20] K. D. Lathrop. Ray effects in discrete ordinates equations. *Nuclear Science and Engineering*, 32(3):357–369, 1968.
- [21] K. D. Lathrop. Remedies for ray effects. *Nuclear Science and Engineering*, 45(3):255–268, 1971.
- [22] C. Lubich and I. V. Oseledets. A projector-splitting integrator for dynamical low-rank approximation. *BIT Numerical Mathematics*, 54(1):171–188, 2014.
- [23] K. A. Mathews. On the propagation of rays in discrete ordinates. *Nuclear science and engineering*, 132(2):155–180, 1999.
- [24] R. G. McClarren, T. M. Evans, R. B. Lowrie, and J. D. Densmore. Semi-implicit time integration for P_n thermal radiative transfer. *Journal of Computational Physics*, 227:7561–7586, 2008.
- [25] R. G. McClarren, J. P. Holloway, and T. A. Brunner. Analytic P_1 solutions for time-dependant, thermal radiative transfer in several geometries. *Journal of Quantitative Spectroscopy and Radiative Transfer*, 109:389–403, 2008.
- [26] R. G. McClarren, J. P. Holloway, and T. A. Brunner. On solutions to the P_n equations for thermal radiative transfer. *Journal of Computational Physics*, 227:2864–2885, 2008.
- [27] J. Morel, T. Wareing, R. Lowrie, and D. Parsons. Analysis of ray-effect mitigation techniques. *Nuclear science and engineering*, 144(1):1–22, 2003.
- [28] G. L. Olson, L. H. Auer, and M. L. Hall. Diffusion, P_1 , and other approximate forms of radiation transport. *Journal of Quantitative Spectroscopy and Radiative Transfer*, 62:619–634, 2000.
- [29] Z. Peng and R. G. McClarren. A high-order/low-order (HOLO) algorithm for preserving conservation in time-dependent low-rank transport calculations. *Journal of Computational Physics*, 447:110672, 2021.
- [30] Z. Peng and R. G. McClarren. A sweep-based low-rank method for the discrete ordinate transport equation. *Journal of Computational Physics*, 473:111748, 2023.
- [31] Z. Peng, R. G. McClarren, and M. Frank. A low-rank method for two-dimensional time-dependent radiation transport calculations. *Journal of Computational Physics*, 421:109735, 2020.
- [32] B. Su and G. L. Olson. An analytical benchmark for non-equilibrium radiative transfer in an isotropically scattering medium. *Annals of Nuclear Energy*, 24(13):1035–1055, 1997.

- [33] J. Tencer. Ray effect mitigation through reference frame rotation. *Journal of Heat Transfer*, 138(11), 2016.